SCIENTIFIC REPORTS

OPEN

Polarization and Thickness Dependent Absorption Properties of Black Phosphorus: New Saturable Absorber for Ultrafast Pulse Generation

Diao Li[1,2,*], Henri Jussila[1,*], Lasse Karvonen[1], Guojun Ye[3,4], Harri Lipsanen[1], Xianhui Chen[3,4,5] & Zhipei Sun[1]

Black phosphorus (BP) has recently been rediscovered as a new and interesting two-dimensional material due to its unique electronic and optical properties. Here, we study the linear and nonlinear optical properties of BP flakes. We observe that both the linear and nonlinear optical properties are anisotropic and can be tuned by the film thickness in BP, completely different from other typical two-dimensional layered materials (e.g., graphene and the most studied transition metal dichalcogenides). We then use the nonlinear optical properties of BP for ultrafast (pulse duration down to ~786 fs in mode-locking) and large-energy (pulse energy up to >18 nJ in Q-switching) pulse generation in fiber lasers at the near-infrared telecommunication band ~1.5 μm. We observe that the output of our BP based pulsed lasers is linearly polarized (with a degree-of-polarization ~98% in mode-locking, >99% in Q-switching, respectively) due to the anisotropic optical property of BP. Our results underscore the relatively large optical nonlinearity of BP with unique polarization and thickness dependence, and its potential for polarized optical pulse generation, paving the way to BP based nonlinear and ultrafast photonic applications (*e.g.*, ultrafast all-optical polarization switches/modulators, frequency converters etc.).

Pulsed laser sources are used in a variety of applications[1–3], ranging from basic research to telecommunications, medicine, and industrial material processing[1–3]. The most-widely used pulsed lasers utilize a Q-switching method or a mode-locking technique[1–3], in which a typical nonlinear optical device, called saturable absorber (SA), turns the continuous wave output of the laser into a periodic train of optical pulses. The SA technology is currently dominated by semiconductor saturable absorber mirrors (SESAMs)[1–3]. However, they typically have limited bandwidth and require complex fabrication and packaging[1]. Recently, carbon nanotubes (CNTs)[4,5] and graphene[6,7] have been demonstrated for SAs with superior performances[8–11], such as broad operation bandwidth[12–14], fast recovery times[15–18], low saturation intensity[4–18], cost-effective and easy fabrication[4–19]. Nevertheless, SAs based on these materials still suffer from drawbacks. For example: when operating at a particular wavelength, CNTs which are not

[1]Department of Micro- and Nanosciences, Aalto University, Tietotie 3, FI-02150 Espoo, Finland. [2]Institute of Photonics & Photo-Technology, Northwest University, Xi'an, 710069, China. [3]Hefei National Laboratory for Physical Science at Microscale and Department of Physics, University of Science and Technology of China, Hefei, 230026, China. [4]Key Laboratory of Strongly-coupled Quantum Matter Physics, University of Science and Technology of China, Chinese Academy of Sciences, Hefei, 230026, China. [5]Collaborative Innovation Center of Advanced Microstructures, Nanjing 210093, China. *These authors contributed equally to this work. Correspondence and requests for materials should be addressed to Z.S. (email: zhipei.sun@aalto.fi)
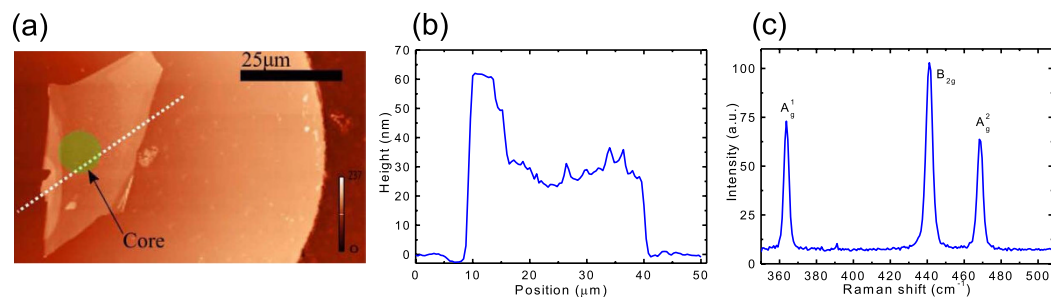
Figure 1. (**a**) AFM image of transferred black phosphorus film on the fiber end. (**b**) Line profile along the dashed white line (marked in (**a**)). The thickness of BP film is ~25 nm at the fiber core (marked with a green circle in (**a**)). (**c**) Raman spectrum of a typical BP film.

in resonance cannot be used, and thereby give relatively large insertion losses[6–8,19]; On the other hand, mono-layer graphene typically has rather weak absorption (~2.3%[20,21]), not suitable for various lasers (*e.g.*, fiber lasers), which typically need relatively larger modulation depth[8–10]; Layered transition metal dichalcogenides (TMDs) (*e.g.*, MoS_2[22], WS_2[23], and $MoSe_2$[24,25]) have also been demonstrated for SAs, but with limited performance for current lasers typically operating at the near-infrared and mid-infrared range, due to their comparatively large bandgap near or in the visible region[26] (~1.8 eV for MoS_2, ~2.1 eV for WS_2, ~1.7 eV for WSe_2[27]).

Black phosphorus (BP), a layered material consisting of only phosphorus atoms, has recently been rediscovered for various applications in electronics and optoelectronics[28–54] (such as transistors, solar cells, and photodetectors). In contrast to graphene and TMDs, BP has its own unique properties[28–54]. For example, its direct electronic band gap can be tuned from ~0.3 to ~2 eV (corresponding to the wavelength range from ~4 to ~0.6 μm), depending on the film thickness[28–54]. This is particularly interesting for photonics, as it can offer a broadly tuneable bandgap with number of layers for the near and mid-infrared photonics and optoelectronics, and thus bridge the present gap between the zero bandgap graphene and the relatively large bandgap TMDs[33].

However, thus far, intensive research efforts on BP have mainly focused on its electronic properties (*e.g.*, transistor performance) and linear optical response (*e.g.*, photo-detector performance). In this paper, we investigate the thickness and polarization dependent linear and nonlinear optical properties of BP thin films, which are integrated into fiber devices, the most commonly-used format for optical telecommunication. Our results show that both linear and nonlinear absorption properties are strongly thickness/polarization dependent, completely different from other typical two-dimensional layer materials (*e.g.*, graphene[8–11] and the most studied TMDs[22–25]). We also demonstrate the use of nonlinear optical property of BP for ultrafast (pulse duration down to ~786 fs in mode-locking) and large-energy (pulse energy up to >18 nJ in Q-switching) pulse generation in fiber lasers at the near-infrared telecommunication band ~1.55 μm. Intriguingly, we observe that the output polarization state of our pulsed fiber lasers is linear (with a degree-of-polarization ~98% in mode-locking, ~99% in Q-switching) due to the unique anisotropic absorption property of BP. These results open the avenue to BP based nonlinear and ultrafast photonic applications (*e.g.*, ultrafast optical switches/modulators, frequency converters etc.).

Results and Discussion

Atomic Force Microscopy and Raman spectroscopy. BP thin films are produced by micromechanical cleavage of a bulk BP crystal, and then transferred to optical fiber ends (details in Methods). The thicknesses of the transferred films on fiber ends are measured by Atomic Force Microscopy (AFM). Figure 1a,b show AFM image taken from a typical BP film and its line profile along the dashed white line. The circular fiber cladding can be resolved from the image, and the location corresponding to the fiber core (marked with the green circle) of a standard single mode fiber (Corning SMF-28, with a core diameter of ~10 microns) is drawn schematically in Fig. 1a. The thickness of the transferred BP film is estimated to be ~25 nm at the location corresponding to the fiber core (Fig. 1b). Typically, the thickness of transferred BP films ranges between ~20 nm and ~1 μm, depending on the micromechanical cleavage process. To verify that the transferred material is BP, we perform polarization-resolved Raman scattering measurements. Raman spectrum of a BP crystal is depicted in Fig. 1c. Three peaks located at the wavenumbers of 363 cm^{-1}, 441 cm^{-1} and 469 cm^{-1} can be observed from the Raman spectrum, and attributed to A_g^1, B_{2g} and A_g^2 vibration modes of BP crystal lattice, respectively. This agrees well with previously published results on BP films[30,31,55]. The Raman peak intensity is also strongly dependent on excitation light polarization (Supplementary Fig. 2) due to its highly anisotropic optical responses[31,45,46], and this has been noted to offer a unique method for determining the crystal orientation of BP films[31,45,46].

Thickness and polarization dependent linear optical absorption. We characterize the linear absorption properties of BP films transferred to the optical fiber ends. The linear transmittance results
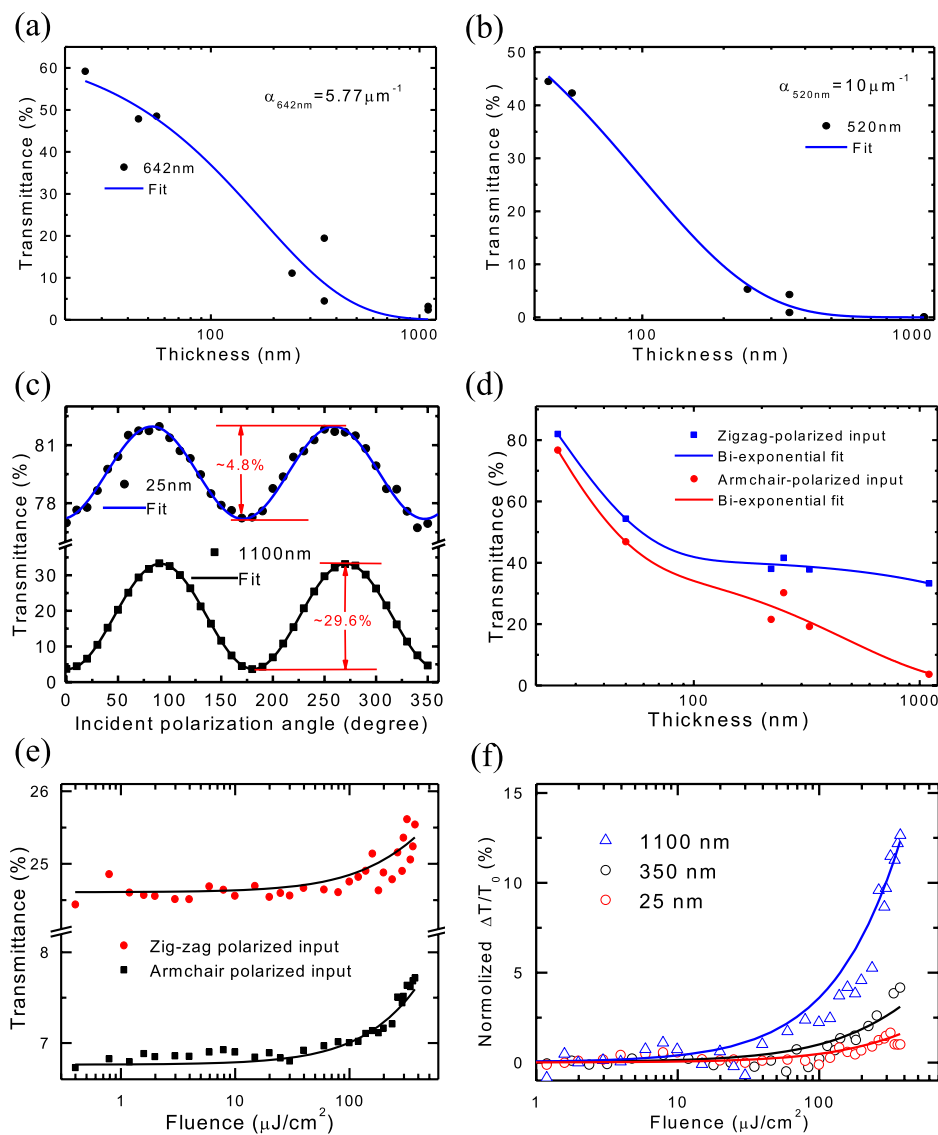
Figure 2. Linear and nonlinear optical properties of BP films: Transmittance of BP films as a function of thickness at the wavelengths of 642 nm (**a**) and 520 nm (**b**). (**c**) Polarization dependent transmittance for 25 nm and 1100 nm thick BP films. The polarization directions corresponding to the maximum and minimum transmittance are linked with the zigzag and armchair axes of BP thin films. (**d**) Transmittance of BP films as a function of film thickness at the wavelength of 1550 nm with two orthogonal polarized light directions. (**e**) Fluence dependent transmittance of the 1100 nm thick BP film measured with ultrafast pulses at two orthogonal polarized light directions. (**f**) Relative transmittance change measured from 25 nm, 350 nm and 1100 nm thick BP films as a function of input pulse fluence. The input polarization direction is along the armchair direction of the BP films.

acquired at 642 nm (~1.93 eV, Fig. 2a) and 520 nm (~2.38 eV, Fig. 2b) show that the transmittance of BP thin films decreases with the film thickness. Note that transmittance includes the contribution from light absorption and reflection. As shown in Fig. 2a,b, the transmittance T agrees well with the fit (solid lines) using the Beer-Lambert law (*i.e.*, $T = \sim \exp(-\alpha \times d)$ where α is the absorption coefficient and d is the film thickness) with the fitted values of $\alpha_{642\,nm} = \sim 5.7\,\mu m^{-1}$, $\alpha_{520\,nm} = \sim 10\,\mu m^{-1}$. These values are comparable to what previously measured and predicted[36]. Thanks to the availability of our polarization-tuneable continuous-wave light source at 1.55 μm (~0.8 eV), we measure the transmittance change of our BP films as a function of incident light polarization angle at this wavelength (*i.e.*, 1.55 μm). The results from 25 nm and 1100 nm thick BP films are given in Fig 2c. It appears that the input light polarization direction strongly affects absorption of the BP film (and thus the transmittance). For instance, we observe that the transmittance of the 1100 nm thick BP film can increase by a factor of >9 (from 3.6% to 33.2%) when

the input polarization direction is altered. It clearly shows the absorption anisotropy of BP[36,37,51,54]. The polarization directions corresponding to the maximum and minimum transmittance are assigned along the zigzag and armchair directions of BP thin films[36,37], respectively. Therefore, such an anisotropic absorption property can be employed to determine the crystal orientation of BP films, similarly to the Raman approach[31,45,46]. Worth noting that this property can be utilized directly for various polarization-based photonic applications (*e.g.*, polarizers).

We find that the polarization dependent transmittance change is significantly larger in thicker samples, which agrees with the recent theoretical simulation[36,37]. For example, the transmittance change (~29.6%) of the 1100 nm thick sample is >6 times larger than the result (~4.8%) of the 25 nm sample (Fig. 2c). Detailed transmittance of samples with variable thicknesses at two orthogonal polarized light directions (Fig. 2d) further confirms that the polarization-introduced transmittance change, which is linked to the selection rules associated with symmetries of the anisotropic material[36,37,54], is thickness dependent. At this wavelength (*i.e.*, 1.55 μm, Fig. 2d), we also observe that the film thickness dependent transmittance matches well with a bi-exponential decay fit which contains two different absorption coefficients, in contrast to the single exponential decay fit of using the Beer-Lambert law at the wavelengths of 642 nm and 520 nm (Fig. 2a,b). As depicted in Fig. 2d, the transmittance decreases first rapidly until the thickness of ~80 nm. After that, the transmittance decreases slowly. The thickness-dependent bandgap (E_g) change of BP has been predicted to follow a power law (*e.g.*, $E_g \approx \frac{1.7\,eV}{n^{0.73}} + 0.3\,eV$, in which n is the number of layers)[36,37,49]. Hence, the change in bandgap attributable to the increasing film thickness can be deduced to be extremely small and will not affect the absorption significantly (compared to the 0.8 eV (~1.55 μm) photon energy used in this experiment), when the sample is thicker than 10 nm. However, it has been calculated that sub-bands close to the bandgap significantly change with the thickness[36,37,43]. Therefore, we assign the rapid decrease in transmittance (when the flake thickness is < 80 nm) mainly to evolution of sub-band energy states[36,37,43] in BP with the film thickness. We believe the Beer-Lambert law dominates the thickness-dependent transmittance change for thicker samples (>~80 nm), similarly to what we observed for the relatively large photon energy transmittance measurement experiments (642 nm in Fig. 2a, and 520 nm in Fig. 2b).

Thickness and polarization dependent nonlinear optical absorption. The nonlinear absorption measurement results are illustrated in Fig. 2e,f. In our measurement setup (Supplementary Fig. 4), we placed a polarization controller before the BP films to adjust the polarization direction of the input ultrafast pulses. Figure 2e depicts the nonlinear absorption measurement results of an 1100-nm thick BP film with two orthogonal polarization directions. A clear increase in the transmittance with the increased pump fluence can be observed in the 1100 nm thick BP sample and is attributed to saturable absorption[43,53]. The polarization dependent nonlinear optical performance difference is also observed in Fig. 2e, which is of great interest for various photonic applications, *e.g.*, tuning operation states in ultrafast lasers[56], switching optical pulses with their polarization directions, and ultrafast vector soliton generations.

Figure 2f shows the relative transmittance change ($\Delta T/T_0$, where ΔT and T_0 are transmittance change and the transmittance at the minimum input power, respectively) for three BP films with the polarization state corresponding to the maximum absorbance (*i.e.*, the armchair-polarized input). Nonlinear saturable absorption is clearly observed in all samples and occurs when the fluence reaches to ~100 μJ/cm². We also note that the thicker sample has ~8-time larger relative transmittance change than the thinner one. This shows that the nonlinear property of BP can be adjusted by the thickness (*i.e.*, number of layers). Such property can be utilized for pulse generation in different laser formats (*e.g.*, fiber and semiconductor lasers), in which nonlinear saturable absorbers with different parameters are needed[8–11].

To estimate the saturation fluence and modulation depth from the nonlinear absorption curves, we use a simplified fluence dependent absorption formula to fit the measurement results (described in Supplementary Information). The fitted curves match decently with the measurement results and are plotted with solid lines in Fig. 2e,f. The obtained saturation fluence from all the samples varies in the range of 2000 μJ/cm² and is, therefore, around an order of magnitude larger than that typically measured with SAs fabricated from CNTs or graphene[7–11,16]. On the other hand, the transmittance change obtained from the measured curves is observed to be larger than 1% (Fig. 2e). However, the modulation depth obtained from the fits typically ranges between 50% and 90%. If true, this observation is promising as the fitted modulation depths are extremely large. However, we note that the fitted modulation depth is probably unrealistically high and most likely relate to the fact that the nonlinear absorption measurement should be continued to larger fluence range which is currently unavailable in our setup. In our nonlinear absorption measurement setup (Supplementary Fig. 4), the available maximum fluence is ~450 μJ/cm².

Q-switched high-energy pulse generation. We use our BP integrated fiber device to build a pulsed fiber laser working at the main telecommunication window of 1.55 μm. Fiber laser is selected in our experiments, as it can offer simple and compact design, efficient heat dissipation, and high-quality pulse generation[57,58]. The layout of our designed fiber laser is schematized in Fig. 3a. A ~1-m Erbium-doped fiber (EDF) is utilized as the gain medium, which is pumped by a 980 nm laser diode (LD) via a wavelength division multiplexer (WDM). A polarization-independent isolator (ISO) is placed after the gain
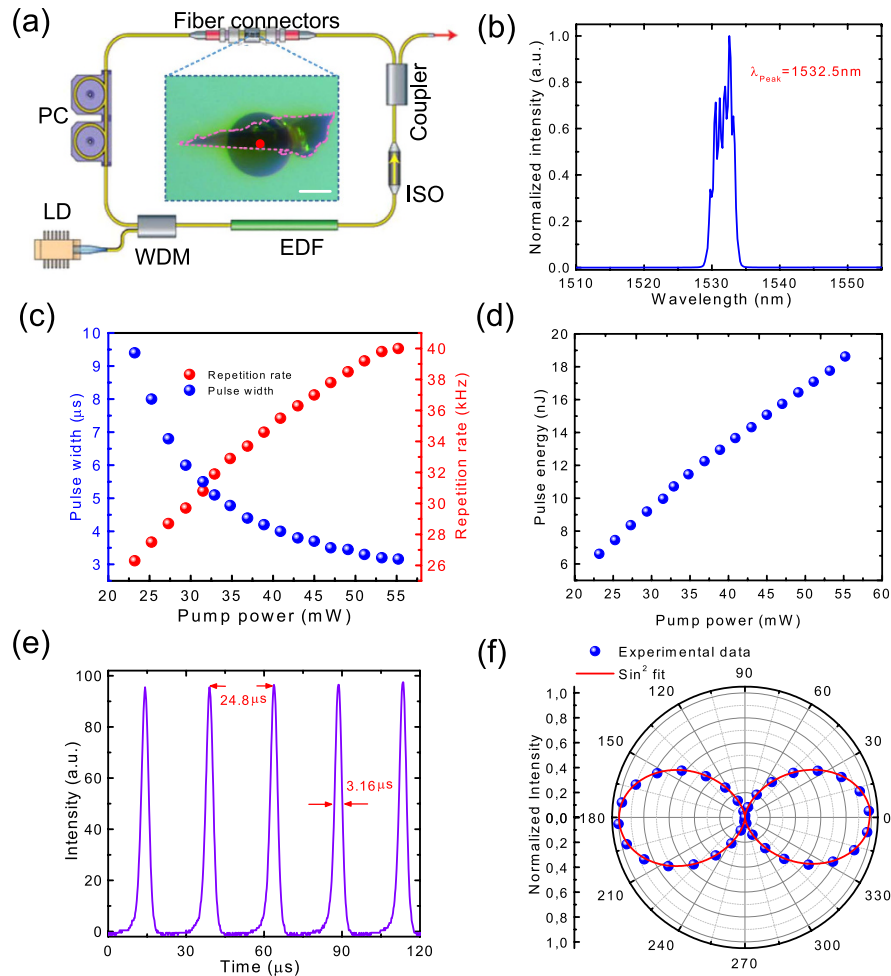
Figure 3. BP Q-switched fiber laser results: (a) Schematic of the laser setup. PC: polarization controller. LD: laser diode. WDM: wavelength division multiplexer. EDF: Erbium-doped fiber. ISO: isolator. The inset shows the transferred BP on the optical fiber end. The scale bar: 60 μm. The red point in the center indicates the ~10 μm-diameter optical fiber core, with the outside concentric grey circle of the 125-μm fiber cladding. The area marked by the pink dotted line specifies the transferred BP. **(b)** Output spectrum. **(c)** Pulse width and repetition rate as a function of pump power. **(d)** Pulse energy as a function of pump power. **(e)** Output pulse train. **(f)** Output polarization property.

fiber to maintain unidirectional operation. A polarization controller (PC) optimizes pulse operation state. A 10/90 coupler is used to extract the light from the cavity for measurements. The total cavity length is ~11 m.

We get Q-switched optical output from the fiber laser, only after inserting the BP integrated device inside the cavity. Q-switching operation is achieved with all BP samples, but the 1100 nm thick BP film gives better performance, as expected from the relatively large transmittance change performance in the device (Fig. 2f). The output performance using the 1100 nm thick BP film is listed in Fig. 3b–f. The threshold pump power for continuous wave lasing is ~11 mW (The output power as a function of pump power is given in Supplementary Fig. 5). When the pump power is increased to ~23 mW, stable Q-switching can be achieved. The peak wavelength is ~1532.5 nm, with the full width at half maximum (FWHM) of ~3 nm (Fig. 3b). The output repetition rate and pulse duration are pump power dependent (Fig. 3c), a typical signature of Q-switching. This is because: when the pump power increases, larger gain is provided to saturate the SA, and thus the repetition rate increases and consequently the pulse duration reduces. In our experiment, the repetition rate increases from ~26 to ~40 kHz, and the pulse duration decreases from ~9.5 to ~3.1 μs, when the pump power is raised from ~23 to ~55 mW. For Q-switched lasers, one of the key parameters is pulse energy, which is also linearly dependent on the pump power, as shown in Fig. 3d. The maximum output pulse energy is ~18.6 nJ. Figure 3e plots a typical pulse train, showing a FWHM pulse-duration of ~3.16 μs, and a pulse period of ~24.8 μs (the corresponding pulse repetition rate is ~40 kHz). The maximum output power in our experiment is 728 μW (Supplementary
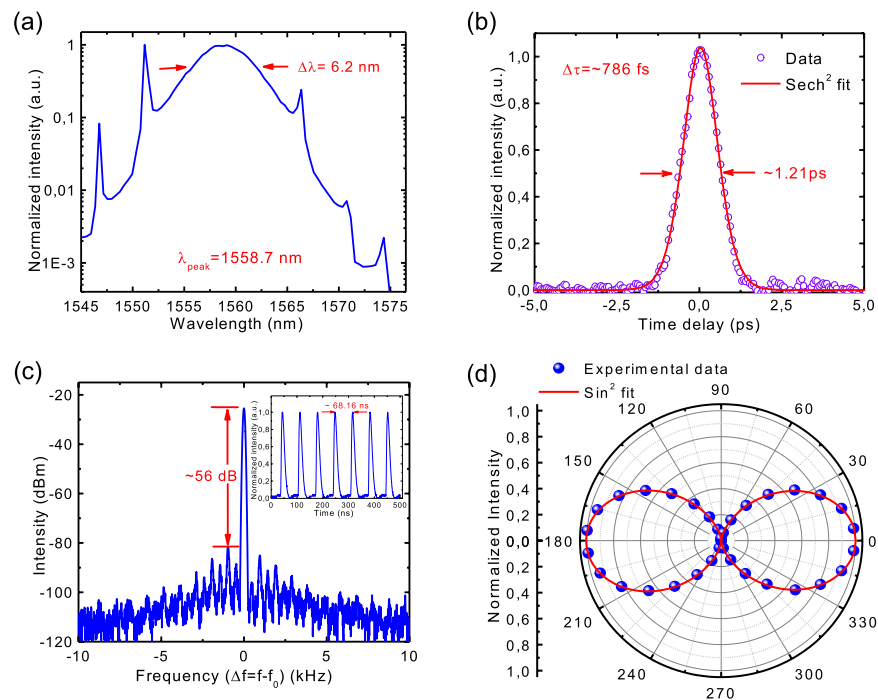
Figure 4. BP mode-locked fiber laser results: (**a**) Output spectrum. (**b**) Output autocorrelation trace, giving a pulse duration of ~786 fs. (**c**) Radio-frequency spectrum at the cavity fundamental repetition rate f_0 ($f_0 = 14.7$ MHz). The resolution bandwidth is 100 Hz. Inset: Output pulse train. (**d**) Output polarization property.

Fig. 5). Note that this output performance is very comparable to typical Erbium-doped fiber lasers Q-switched with other nanomaterials (*e.g.*, CNTs and graphene[8–11]).

Then, we further examine the output polarization property of our Q-switched BP fiber laser (shown in Fig. 3f) by placing a rotatable polarizer plate between the laser output end and the power meter (the measurement setup is given in Supplementary Fig. 7). Interestingly, we observe that the output pulses of the laser can be perfectly linearly-polarized. The degree-of-polarization (DOP) (DOP = $(P_{max} - P_{min})$/ $(P_{max} + P_{min})$, where P_{max} and P_{min} are the maximum and minimum power measured, respectively)[56] of the linearly-polarized output is ~99%. The linear polarization output of our BP fiber laser is attributed to the anisotropic absorption in the BP saturable absorber (shown in Fig. 2f).

Mode-locked ultrafast pulse generation. When the fiber cavity length is increased to ~14.2 meters (after adding ~3 m of SMF-28 single mode fiber in the laser cavity), the total group velocity dispersion of our fiber cavity is $\sim -2.5 \times 10^{-1}$ ps^2. In this case, it can facilitate soliton-like pulse shaping through the interplay of group velocity dispersion and self-phase modulation[58]. Indeed, after inserting our BP integrated fiber device in this fiber cavity, stable mode-locking can be initiated by introducing a disturbance to the intra-cavity fiber. Once stable output is achieved, no further polarization controller adjustment is required. The output power is ~1.6 mW when the pump power is 68.9 mW. Figure 4 summarizes the mode-locked laser performance. The laser mode-locks at 1558.7 nm, with the FWHM of 6.2 nm. The side bands (at 1546.76, 1551.16, 1566.36, 1570.76, and 1574.36 nm, shown in Fig. 4a) fully confirm our soliton-like mode-locking, as they are typical for soliton-like pulse formation, resulting from intra-cavity periodical perturbations of discrete loss, gain and dispersion[59]. Figure 4b gives a typical output auto-correlation trace, which is well fitted by a sech^2 temporal profile. The pulse duration is ~786 fs. The time-bandwidth product (TBP) of the mode-locked pulses is ~0.6. The deviation from the TBP value of ~0.315 anticipated for transform-limited sech^2 pulses suggests the presence of chirping of the generated ultrafast pulses[58]. Shorter pulses may be obtained by using fiber lasers with specifically-design dispersion map (*e.g.*, stretched-pulse fiber laser design[15,17,60]).

To investigate the laser output stability[61,62], we characterize the radio frequency spectrum. We first measure broad-span frequency spectrum up to 500 MHz (Supplementary Fig. 6). It presents no significant spectral modulation, implying no Q-switching instabilities[61,62]. Figure 4c gives the radio frequency spectrum around the fundamental repetition rate (f_0). A >50 dB signal-to-background ratio (corresponding to $>10^5$ contrast) is observed, showing good mode-locking stability[61,62]. The inset of Fig. 4c depicts the

output pulse train, with a period of 68.16 ns, corresponding to the cavity fundamental repetition rate f_0 of 14.7 MHz, as expected from the total fiber cavity length of ~14.2 meters.

We also measure the output polarization property of our mode-locked BP fiber laser with the method identical to the polarization measurement setup used for the Q-switched laser (see Supplementary Fig. 7). We observe that the polarization state of the mode-locked BP fiber laser is also linearly polarized, as shown in Fig. 4d. The DOP is ~98%. Such linearly-polarized output is also attributed to the anisotropic absorption in BP saturable absorber, which is different from other commonly used saturable absorber materials such as graphene and SESAMs.

Note that the performance of the BP mode-locked laser (output power level, repetition rate, pulse duration, etc.) is comparable to what was typically achieved with CNTs and graphene based fiber lasers[6–11]. However, given the unique bandgap tuning property from visible to mid-infrared range, we expect superior performance of BP thin films for ultrafast lasers at this spectral range, worthy of future research. Particularly, the unique polarization/thickness dependent optical properties of BP studied here, are completely different from that of other typical two-dimensional layer materials (e.g., graphene[8–11] and the most studied TMDs[22–25]). This can potentially introduce paradigms of novel optical devices for both linear (e.g., polarization dynamics control) and nonlinear photonic applications (e.g., ultrafast linearly-polarized pulse generation[63]). For example, the thickness dependent property offers a tunability to the effective response spectrum due to the layer controlled direct band gap; the anisotropic absorption property can provide an effective method to tune the output polarization state in laser applications.

In summary, we have studied the thickness and polarization dependent linear and nonlinear optical properties of BP thin films, and then utilized their nonlinear anisotropic absorption property to generate ultrafast and large-energy linearly-polarized pulses with BP integrated fiber devices. Our results exhibit the practical potential of this promising material for various nonlinear and ultrafast photonic and optoelectronic applications.

During the preparation of this paper, we became aware of two experimental works studying pulsed fiber lasers with BP on arXiv.org (arXiv: 1504.04731, arXiv: 1505.03035).

Methods

BP device fabrication.   BP was synthesized under a constant pressure of 10 kbar by heating red phosphorus to 1,000 °C and slowly cooling to 600 °C at a cooling rate of 100 °C per hour. Red phosphorus was purchased from Aladdin Industrial Corporation with 99.999% metals basis. The high-pressure environment was provided by a cubic-anvil-type apparatus (Riken CAP-07). After that, BP films were produced by micromechanical cleavage of bulk BP crystals directly onto a viscoelastic polydimethylsiloxane (PDMS) stamp. A selected BP film on the PDMS stamp is then placed on a fiber end with the help of optical microscope and micromanipulator. Due to viscoelastic properties of PDMS, the BP film adheres to the fiber end when the PDMS stamp is gently lifted off[47,48].

AFM and Raman spectroscopy.   AFM measurements were performed in semi-contact mode using NTegra Aura AFM apparatus equipped with a scanning head. A custom-made measurement stage was fabricated allowing us to characterize the BP films attached on the fiber end. The maximum scan size of the setup was $100 \times 100\,\mu m^2$. Raman spectra were performed by using a confocal Raman microscope (Witec alpha 300 R) equipped with a frequency doubled Nd:YAG green laser ($\lambda = 532$ nm). The samples were placed on the SiO_2/Si substrate, fabricated with the same fabrication approach discussed above, and the thicknesses of the characterized films were measured by AFM.

Linear absorption measurement.   A home-made erbium-doped fiber based amplified spontaneous emission source was used to characterize the absorption spectrum from ~1500 to 1600 nm. Its output polarization was changed with a prism based polarizer to measure the polarization dependent transmittance. Absorption properties at different wavelengths (e.g., 520, 642 nm) were measured with various fiber coupled non-polarized laser diodes (i.e., without polarization-tuning capability). The input power for the linear absorption measurement was set less than 1 mW.

Nonlinear absorption measurement.   A power-amplified home-made ultrafast fiber laser (~15 mW, 530 fs, 62 MHz) was employed to measure the saturable absorption property of the BP based fiber devices. A polarization controller was used to change the light polarization direction to measure polarization dependent saturable absorption performance. A double channel power meter (Ophir, Laserstar) was used to achieve high-accuracy measurement.

Laser characterization.   An optical spectrum analyser (Anritsu, MS9740A), a power meter (Ophir, Nova II), and a second-harmonic generation autocorrelator (APE, Pulse-check50) were used to characterize the generated ultrafast pulse performance. Pulse train was measured by an oscilloscope connected with a photodetector, while the radio frequency spectrum was taken by a radio frequency analyser (Anritsu MS2692A) with an ultrafast (>25 GHz) photodetector.

References

1. Keller U. Recent developments in compact ultrafast lasers. *Nature* **424,** 831–838 (2003).
2. Dausinger, F., Lichtner, F. & Lubatschowski, H. *Femtosecond Technology for Technical and Medical Applications.* (Springer, 2004).
3. Fermann, M. E., Galvanauskas, A. & Sucha, G. *Ultrafast Lasers Technology and Applications.* (Marcel Dekker, 2003).
4. Set, S. Y., Yaguchi, H., Tanaka, Y. & Jablonski, M. Laser mode locking using a saturable absorber incorporating carbon nanotubes. *J. Lightwave Technol.* **22,** 51–56 (2004).
5. Hasan, T. *et al.* Double Wall Carbon Nanotubes for Wide-Band, Ultrafast Pulse Generation. *ACS Nano* **8,** 4836–4847 (2014).
6. Hasan, T. *et al.* Nanotube-Polymer Composites for Ultrafast Photonics. *Adv. Mater.* **21,** 3874–3899 (2009).
7. Bao, Q. *et al.* Atomic-Layer Graphene as a Saturable Absorber for Ultrafast Pulsed Lasers. *Adv. Funct. Mater.* **19,** 3077–3083 (2009).
8. Bonaccorso, F., Sun, Z., Hasan, T. & Ferrari, A. C. Graphene Photonics and Optoelectronics. *Nat. Photonics* **4,** 611–622 (2010).
9. Sun, Z., Hasan, T. & Ferrari, A. C. Ultrafast lasers mode-locked by nanotubes and graphene. *Physica E* **44,** 1082–1091 (2012).
10. Yamashita, S. A Tutorial on Nonlinear Photonic Applications of Carbon Nanotube and Graphene. *J. Lightwave Technol.* **30,** 427–447 (2012).
11. Martinez, A. & Sun, Z. Nanotube and graphene saturable absorbers for fibre lasers. *Nat. Photonics* **7,** 842–845 (2013).
12. Wang, F. *et al.* Wideband-tuneable, nanotube mode-locked, fibre laser. *Nat. Nanotechnol.* **3,** 738–742 (2008).
13. Sun, Z. *et al.* A stable, wideband tunable, near transform-limited, graphene-mode-locked, ultrafast laser. *Nano Res.* **3,** 653–660 (2010).
14. Fu, B. *et al.* Broadband Graphene Saturable Absorber for Pulsed Fiber Lasers at 1, 1.5 and 2 um. *IEEE J. Sel. Top. Quantum Electron.* **20,** 1100705 (2014).
15. Popa, D. *et al.* 74-fs nanotube-mode-locked fiber laser. *Appl. Phys. Lett.* **101,** 153107 (2012).
16. Cho, W. B. *et al.* Boosting the Non Linear Optical Response of Carbon Nanotube Saturable Absorbers for Broadband Mode-Locking of Bulk Lasers. *Adv. Funct. Mater.* **20,** 1937–1943 (2010).
17. Popa, D. *et al.* Sub 200fs pulse generation from a graphene mode-locked fiber laser. *Appl. Phys. Lett.* **97,** 203106 (2010).
18. Tarka, J. *et al.* 168 fs pulse generation from graphene-chitosan mode-locked fiber laser. *Opt. Mater. Exp.* **4,** 1981–1986 (2014).
19. Sun, Z. *et al.* Graphene Mode-Locked Ultrafast Laser. *ACS Nano* **4,** 803–810 (2010).
20. Nair, R. R. *et al.* Fine Structure Constant Defines Visual Transparency of Graphene. *Science* **320,** 1308–1308 (2008).
21. Mak, K. F. *et al.* Measurement of the Optical Conductivity of Graphene. *Phys. Rev. Lett.* **101,** 196405 (2008).
22. Zhang, H. *et al.* Molybdenum disulfide (MoS_2) as a broadband saturable absorber for ultra-fast photonics. *Opt. Express* **22,** 7249–7260 (2014).
23. Mao, D. *et al.* WS_2 mode-locked ultrafast fiber laser. *Sci. Rep.* **5,** 7965 (2015).
24. Luo, Z. *et al.* Nonlinear optical absorption of few-layer molybdenum diselenide ($MoSe_2$) for passively mode-locked soliton fiber laser. *Photon. Research* **4,** 231765 (2015).
25. Woodward, R. I. *et al.* Wideband saturable absorption in few-layer molybdenum diselenide ($MoSe_2$) for Q-switching Yb-, Er- and Tm-doped fiber lasers. *arXiv* 1503.08003 (2015).
26. Bonaccorso, F. & Sun, Z. Solution processing of graphene, topological insulators and other 2d crystals forultrafast photonics. *Opt. Mater. Exp.* **4,** 63–78 (2014).
27. Wang, Q. H., Kalantar-Zadeh, K., Kis, A., Coleman, J. N. & Strano, M. S. Electronics and optoelectronics of two-dimensional transition metal dichalcogenides. *Nat. Nanotechnol.* **7,** 699–712 (2012).
28. Li, L. *et al.* Black phosphorus field-effect transistors. *Nat. Nanotechnol.* **9,** 372–377 (2014).
29. Deng, Y. *et al.* Black Phosphorus–Monolayer MoS_2 van der Waals Heterojunction p–n Diode. *ACS Nano* **8,** 8292–8299 (2014).
30. Liu, H. *et al.* Phosphorene: An Unexplored 2D Semiconductor with a High Hole Mobility. *ACS Nano* **8,** 4033–4041 (2014).
31. Xia, F., Wang, H. & Jia, Y. Rediscovering black phosphorus as an anisotropic layered material for optoelectronics and electronics. *Nat. Commun.* **5,** 54458 (2014).
32. Koenig, S. P., Doganov, R. A., Schmidt, H., Castro Neto, A. H. & Özyilmaz, B. Electric field effect in ultrathin black phosphorus. *Appl. Phys. Lett.* **104,** 103106 (2014).
33. Ling, X., Wang, H., Huang, S., Xia, F. & Dresselhaus, M. S. The renaissance of black phosphorus. *PNAS,* **112,** 4523 (2015).
34. Buscema, M., Groenendijk, D. J., Steele, G. A., van der Zant, H. S. J. & Castellanos-Gomez, A. Photovoltaic effect in few-layer black phosphorus PN junctions defined by local electrostatic gating. *Nat. Commun.* **5,** 4651 (2014).
35. Kang, J. *et al.* Solvent Exfoliation of Electronic-Grade, Two-Dimensional Black Phosphorus. *ACS Nano* **9,** 3596–3604 (2015).
36. Low, T. *et al.* Tunable optical properties of multilayer black phosphorus thin films. *Phys. Rev. B* **90,** 075434 (2014).
37. Tran, V., Soklaski, R., Liang, Y. & Yang, L. Layer-controlled band gap and anisotropic excitons in few-layer black phosphorus. *Phys. Rev. B* **89,** 235319 (2014).
38. Hong, T. *et al.* Polarized photocurrent response in black phosphorus field-effect transistors. *Nanoscale* **6,** 8978–8983 (2014).
39. Liu, H., Du, Y., Deng, Y. & Ye, P. D. Semiconducting black phosphorus: synthesis, transport properties and electronic applications. *Chem. Soc. Rev.* **44,** 2732 (2015).
40. Yasaei, P. *et al.* High-Quality Black Phosphorus Atomic Layers by Liquid-Phase Exfoliation. *Adv. Mater.* **27,** 1887 (2015).
41. Buscema, M. *et al.* Fast and Broadband Photoresponse of Few-Layer Black Phosphorus Field-Effect Transistors. *Nano Lett.* **14,** 3347–3352 (2014).
42. Xia, F., Wang, H., Xiao, D., Dubey, M. & Ramasubramaniam, A. Two-dimensional material nanophotonics. *Nat. Photonics* **8,** 899–907 (2014).
43. Qiao, J., Kong, X., Hu, Z.-X., Yang, F. & Ji, W. High-mobility transport anisotropy and linear dichroism in few-layer black phosphorus *Nat. Commun.* **5,** (2014).
44. Ge, S. *et al.* Dynamical Evolution of Anisotropic Response in Black Phosphorus under Ultrafast Photoexcitation. *arXiv* 1503.08524 (2015).
45. Zhang, S. *et al.* Extraordinary Photoluminescence and Strong Temperature/Angle-Dependent Raman Responses in Few-Layer Phosphorene. *ACS Nano* **8,** 9590–9596 (2014).
46. Ribeiro, H. B. *et al.* Unusual Angular Dependence of the Raman Response in Black Phosphorus. *ACS Nano* **9,** 4270–4276 (2015).
47. Andres, C.-G. *et al.* Isolation and characterization of few-layer black phosphorus. *2D Materials* **1,** 025001 (2014).
48. Andres, C.-G. *et al.* Deterministic transfer of two-dimensional materials by all-dry viscoelastic stamping. *2D Materials* **1,** 011002 (2014).
49. Das, S. *et al.* Tunable Transport Gap in Phosphorene. *Nano Lett.* **14,** 5733–5739 (2014).
50. Youngblood, N., Chen, C., Koester, S. J. & Li, M. Waveguide-integrated black phosphorus photodetector with high responsivity and low dark current. *Nat. Photonics* **9,** 247–252 (2015).
51. Wang, X. *et al.* Highly Anisotropic and Robust Excitons in Monolayer Black Phosphorus. *Nat. Nano.* **10,** 517 (2015).
52. Reich, E. S. Phosphorene excites materials scientists. *Nature* **506,** 19 (2014).
53. Lu, S. B. *et al.* Broadband nonlinear optical response in multi-layer black phosphorus: an emerging infrared and mid-infrared optical material. *Opt. Express* **23,** 11183–11194 (2015).
54. Yuan, H. *et al.* Broadband Linear-Dichroic Photodetector in a Black Phosphorus Vertical p-n Junction. *arXiv* 1409.4729 (2014).

55. Sugai, S. & Shirotani, I. Raman and infrared reflection spectroscopy in black phosphorus. *Solid State Comm.* **53,** 753–755 (1985).
56. Yang, H. *et al.* Broadband laser polarization control with aligned carbon nanotubes, *Nanoscale*, **7,** 11199 (2015).
57. Okhotnikov, O., Grudinin, A. & Pessa, M. Ultra-fast fibre laser systems based on SESAM technology: new horizons and applications. *New J. Phys.* **6,** 177 (2004).
58. Agrawal, G. P. *Applications of Nonlinear Fiber Optics.* (Academic, 2001).
59. Dennis, M. L. & Duling, I. N. Experimental study of sideband generation in femtosecond fiber lasers. *IEEE J. Quantum Electron.* **30,** 1469–1477 (1994).
60. Tamura, K., Ippen, E. P., Haus, H. A. & Nelson, L. E. 77-fs Pulse Generation From a Stretched-pulse Mode-locked All-fiber Ring Laser. *Opt. Lett.* **18,** 1080–1082 (1993).
61. Von der Linde, D. Characterization of the Noise in Continuously Operating Mode-Locked Lasers. *Appl. Phys. B* **39,** 201–217 (1986).
62. Honninger, C., Paschotta, R., Morier-Genoud, F., Moser, M. & Keller, U. Q-switching stability limits of continuous-wave passive mode locking. *J. Opt. Soc. Am. B* **16,** 46–56 (1999).
63. Sergeyev, S. V., Mou, C., Rozhin, A. & Turitsyn, S. K. Vector solitons with locked and precessing states of polarization. *Opt. Express* **20,** 27434–27440 (2012).

Author Contributions

Z.S. conceived the experiments. Z.S., D.L., H.J. and L.K. designed the experiments. H.J. performed device fabrication and AFM measurement. D.L. performed optical measurements. L.K. performed Raman measurement. G.Y. and X.C. grew the high quality BP crystals. All authors contribute to data discussions.

Additional Information

Supplementary information accompanies this paper at http://www.nature.com/srep

Competing financial interests: The authors declare no competing financial interests.

How to cite this article: Li, D. *et al.* Polarization and Thickness Dependent Absorption Properties of Black Phosphorus: New Saturable Absorber for Ultrafast Pulse Generation. *Sci. Rep.* **5**, 15899; doi: 10.1038/srep15899 (2015).